JOURNAL OF MATERIALS SCIENCE 31 (1996) 1415–1423

The strain-rate and temperature dependence of the mechanical properties of polyetherketone and polyetheretherketone

S. HAMDAN*, G. M. SWALLOWE
Department of Physics, Loughborough University of Technology, Leicestershire LE11 3TU, UK

The mechanical properties of polyetheretherketone and polyetherketone were studied as a function of strain rate and temperature in the ranges 10^{-3} to $10^{3}\,s^{-1}$ and 20–200 °C. At temperatures below the glass transition temperature, T_g, the strain-rate sensitivity of both polymers was found to be almost independent of temperature with a value of ~4 MPa per decade of strain rate and the behaviour was well described by an Eyring relationship leading to an activation volume of ~1 nm^3. Above T_g, X-ray and differential scanning calorimetry studies show that cold-crystallization phenomena play a very important part in the polymer behaviour, leading to an increase of yield stress with increasing temperature. The crystallization was found to be highly strain-rate dependent with no increase in crystalline content occurring in quasi-static tests and increases of up to 20% in higher rate tests. Much of the data have been gathered using novel test equipment which is described in the paper.

1. Introduction

Polyetheretherketone (PEEK) is a thermoplastic resin of some interest to certain elements of the aerospace industry. The synthesis of this family of polymers has been described by Attwood *et al.* [1]. It has a repeat unit of three aromatic rings separated by two ethers and one carbonyl group in that order. The glass transition and melting point are about 144 and 335° C, respectively, and they were studied by Cheng *et al.* [2].

Polyetherketone (PEK) has a remarkably high glass transition temperature of about 162 °C and a melting point of 373 °C. Its structure comprises two aromatic rings separated by an ether and a carbonyl group. The crystal structure of PEEK is orthorhombic [3, 4]. The crystalline morphologies of PEEK solidified from the melt were studied by Blundell and Osborn [5] and the crystallization behaviour of PEEK has been studied both under isothermal and non-isothermal conditions [6, 7]. The effects of crystallinity and temperature on the mechanical properties of PEEK have also been studied by Lee *et al.* [8]. They found that crystallinity in PEEK increases with annealing temperature up to a maximum of 28%, with a melting point at 335 °C.

In this paper, we report the mechanical properties of PEEK and PEK using a range of mechanical testing machines, all employing a compression test on cylindrical samples of the same dimensions throughout. Two testing machines are particularly novel to mechanical testing in general, and are substantially different from previously adopted test methods for polymers.

In this work, the compressive properties of PEEK and PEK were studied over the temperature range 20–200 °C at strain rates ranging from 10^{-3} to $10^{3}\,s^{-1}$. Because PEEK and PEK can be quenched to an amorphous glass, or crystallized over a wide temperature range, they are interesting materials in which to study the interplay of morphology and mechanical properties. Central to such a study is the establishment of the degree of crystallinity. The various effects of crystallinity on mechanical properties could be important in determining the stress response of PEEK as a matrix in composites.

Because the testing temperature and degree of crystallinity affected the compressive properties, the annealed samples before and after mechanical testing were characterized using wide-angle X-ray diffraction (WAXD) and differential scanning calorimetry (DSC). Differential calorimetry scanning on the tested samples indicates that crystal formation occurs simultaneously with textural orientation, as determined from X-ray diffraction.

2. Experimental procedure

2.1. Samples

Commercial plaques of PEEK and PEK (grade 150G and 220G, respectively) manufactured by ICI Plastics Ltd, UK, were used as-received. All samples of each material were manufactured from the same batch of material. The samples were machined on a lathe from a single plate, 3.5 mm thick. Their configuration, as

*Present address: Department of Physics, University Pertanian Malaysia, Serdang 43400, Selangor, Malaysia.

0022–2461

recommended by many workers [9], was a short cylinder of 7.0 mm diameter and thickness 3.5 mm, i.e. diameter/height ratio = 2.

2.2. Low strain-rate tests

Mechanical testing was done on a Dartec hydraulic machine operating at strain rate of order 10^{-3} to $10^{1}\ s^{-1}$. The lower jaw of the machine was equipped with an iron block heater controlled by a thermostat. Tests were performed at a constant crosshead speed from room temperature to 200 °C in steps of 20 °C. Strain was computed from crosshead movement and samples were taken to 60% strain. Force was measured by a load cell attached to the upper jaw of the machine. Stress was calculated based on the expanding area of the samples, assuming that the sample volume remains constant.

2.3. Medium and high strain-rate tests

A conventional dropweight system was used to determine the stress–strain properties at rates of order $10^{2}\ s^{-1}$. Force was measured via a strain-gauged anvil. The system was essentially the same as that described by Field *et al.* [10] with the exception that the axial displacement, and thus axial strain, was measured directly via the intensity reduction of a laser beam targeted on a wide-area photodiode (Fig. 1) by a flag attached to the dropping weight. Assuming deformation was homogeneous and volume was conserved, the expanding area of the deformed sample could be calculated from the axial displacement and therefore stress determined from the measured force and calculated area. This avoided the inaccuracies inherent in the method of strain determination from double integration of the force–time trace [10].

Stress–strain measurements were also made using a novel method which consisted of a dropweight system operating at $10^{3}\ s^{-1}$ and incorporated a high-speed A.W.R.E. C4 camera. This system measured force via an accelerometer attached to the dropping weight while the radial displacement and thus radial strain was measured via the photographs captured by the camera (Fig. 2). A light path through the weight and glass anvils enabled the photographs to be taken. The sample was viewed by transmitted light from a flash unit triggered by the falling weight. The camera was able to capture 140 frames with a minimum interframe interval of 7 μs. A major advantage of the system is the ability to observe directly and to correlate sample behaviour with the applied stress.

In this system, synchronization of the force from the accelerometer with the high-speed camera images is very critical. Triggering of the flash unit which produces the first camera image also produces a sharp spike on the accelerometer output trace. This spike is used to synchronize the accelerometer output with the first camera image. Knowing the rotation speed and thus the interframe time, subsequent frames can be correlated with the accelerometer signal. Because the accelerometer is attached to the top of the dropweight, the time delay for the stress pulse to travel between the

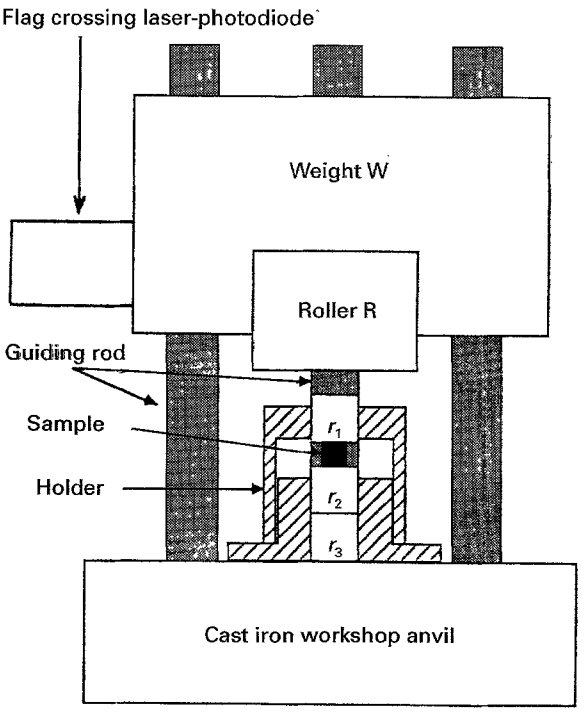

Figure 1 Conventional dropweight system configuration.

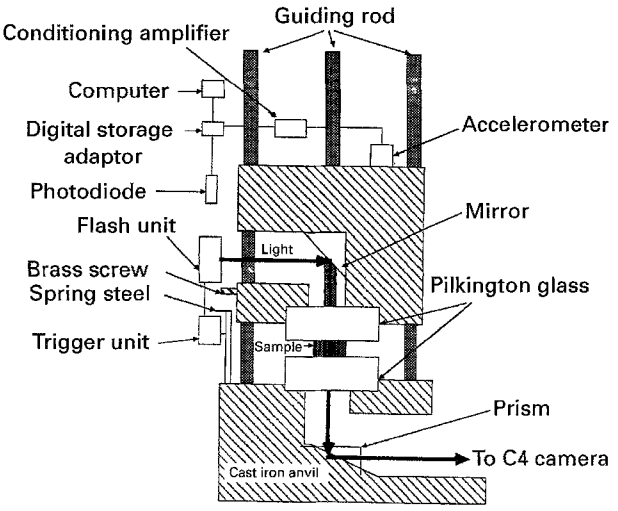

Figure 2 Improved dropweight system configuration.

point of impact and the point of signal detection has also been incorporated into the calculation.

After being processed, the film was enlarged using a slide projector and the diameter of the sample measured. These photographs gave direct measurements of the expanding area of the deformed sample. These measured areas, combined with the force from the accelerometer, yielded direct stress measurements. In this system, axial strain was inferred from the radial strain assuming the deformation is homogeneous and volume always conserved.

Owing to the unusual geometry of the system, the signal derived from an impact test on the glass anvil was distorted by extraneous vibrations. In this work, the transient stress pulses which may contain contributions from the measuring systems were transformed to the frequency domain where a correction for these dynamic effects was performed. Digital filtering using

the MATHCAD Numerical Analysis package on a personal computer was used on the original unfiltered data. Because the frequencies of the vibrations due to the system were all above 30 kHz and the stress pulse components were mainly in the region 1–20 kHz, the high frequency vibration was removed above a threshold value. Inverse transformation then yielded the true stress pulse.

The fourth system used in the work was a cross-bow system. This system gives strain rates of the order $10^3\ s^{-1}$ and operates like the direct-impact Hopkinson pressure bar described by Gorham [11]. In this system, force can be detected via an instrumented pressure bar which is calibrated independently using a conventional split Hopkinson pressure bar (SHPB) system. The axial displacement is measured using the reduction in intensity of a laser beam targeted on a wide area photodiode with the flag attached to the input bar (similar to the dropweight system above). The input bar is used merely as a base to carry the strain-measuring flag. Force is applied to the input bar by means of a metal arrow in the form of a long solid cylinder. This system is schematically illustrated in Fig. 3.

2.4. Sample characterization

A Mettler DSC20 differential scanning calorimeter interfaced to a BBC computer was used to determine the thermal characteristics of PEEK and PEK, using procedures detailed elsewhere [12]. A Philips PW1130/00 generator with a PW2233/20 copper X-ray tube was used to record the WAXD patterns in reflection mode using CuK_α radiation. Accurate peak positions were determined on both tested and untested samples using an automatic powder diffractometer.

3. Results and discussion

3.1. Mechanical testing

Fig. 4 illustrates the results of mechanical testing on PEEK and PEK at quasi-static rate ($10^{-3}\ s^{-1}$) from 20–200 °C. Samples were heated to the desired temperature and allowed to stand for 30 min to reach equilibrium temperature before each test. The curves clearly show strain hardening after yield. As the testing temperature increases, the yield stress and flow stress decrease.

Thermal history imparted to semicrystalline polymer in mechanical testing at $7\ s^{-1}$ affects the stress–strain properties significantly for testing above T_g (see Fig. 5). In this test, the yield and flow stresses

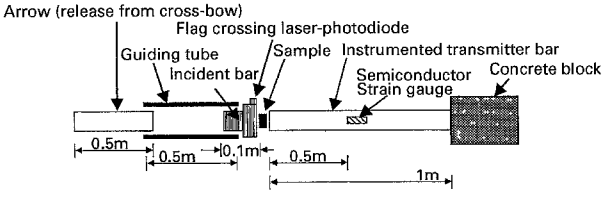

Figure 3 Cross-bow system configuration.

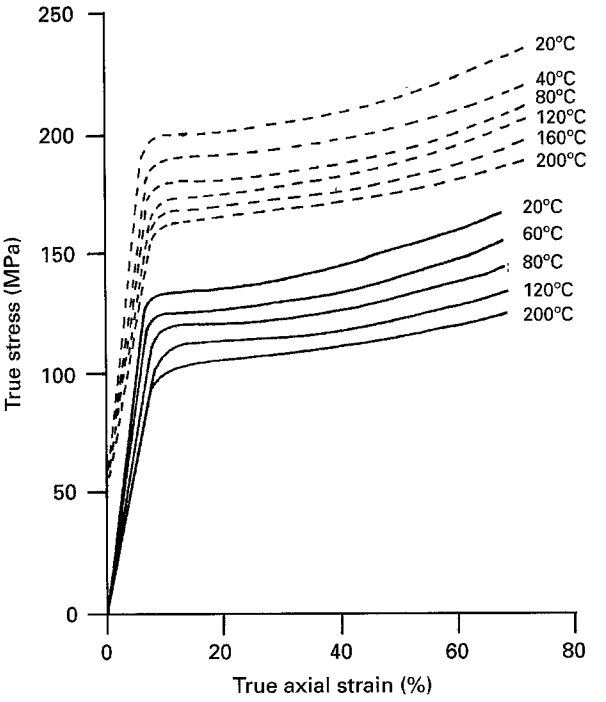

Figure 4 True stress against true axial strain for (——) PEEK and (- - - -) PEK from quasi-static tests ($10^{-3}\ s^{-1}$) at 20–200 °C. The PEK data have been offset by 50 MPa.

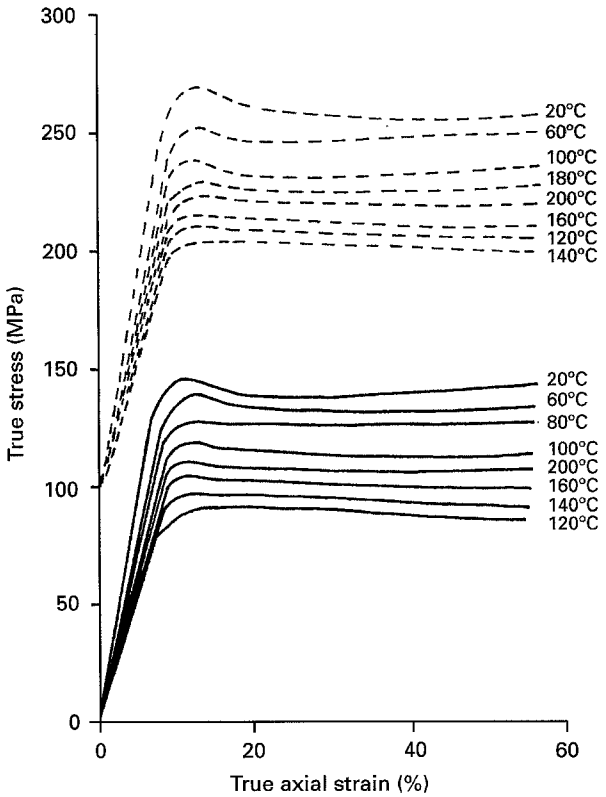

Figure 5 True stress against true axial strain for (——) PEEK and (- - - -) PEK from dynamic tests ($7\ s^{-1}$) at 20–200 °C. The PEK data have been offset by 100 MPa.

increase with temperature for tests at temperatures above T_g. These findings agree very well with the work of Lee *et al.* [8]. Tables I and II show the yield stress and flow stress as a function of the annealing temperature. Note that in this work, samples were held at the test temperature for 30 min before testing. The test

TABLE I Variation of stress with temperature at yield and 20% strain measured from the stress–strain curve of PEEK tested at 3×10^{-3} and $7\ s^{-1}$

Testing temperature (°C)	$3 \times 10^{-3}\ s^{-1}$		$7\ s^{-1}$	
	σ_{yield} (MPa)	$\sigma_{20\%\varepsilon}$ (MPa)	σ_{yield} (MPa)	$\sigma_{20\%\varepsilon}$ (MPa)
20	132	137	150	145
40	130	135	144	142
60	123	128	138	136
80	117	122	118	126
100	106	113	114	120
120	109	114	98	100
140	106	110	93	97
160	102	108	97	102
180	99	102	100	104
200	100	106	102	106

TABLE II Variation of stress with temperature at yield and 20% strain measured from the stress–strain curve of PEK tested at $3 \times 10^{-3} s^{-1}$ and $7\ s^{-1}$

Testing temperature (°C)	$3 \times 10^{-3}\ s^{-1}$		$7\ s^{-1}$	
	σ_{yield} (MPa)	$\sigma_{20\%\varepsilon}$ (MPa)	σ_{yield} (MPa)	$\sigma_{20\%\varepsilon}$ (MPa)
20	150	152	170	163
40	139	142	163	154
60	133	135	150	148
80	128	133	147	145
100	113	120	137	134
120	120	126	107	109
140	109	112	110	114
160	113	120	116	117
180	116	120	120	124
200	112	118	115	120

temperature was therefore equivalent to an annealing temperature. Apparently, the yield strength of PEEK and PEK is a direct function of crystalline morphology.

Between room temperature and T_g the flow stress decreases with increasing temperature. The heat treatment above T_g results in a high degree of crystallinity and crystal perfection, which imparts toughness, and increase in the yield and flow stress as is also evinced from tests at $500\ s^{-1}$ (Fig. 6).

Figs 7 and 8 show the results from the improved dropweight and cross-bow systems, respectively. Because as-received samples have very nearly the same degree of crystallinity, the differences in the flow stress with annealing temperature must be associated with the degree of crystalline perfection resulting from the heating temperature. The effect of these more perfect crystals is seen in the increased stresses for plastic flow in the annealed samples above T_g. Table III shows the effect of strain rate on the yield strength of PEEK and PEK. Fig. 9 shows the stress–strain curves for PEEK and PEK obtained at five different strain rates.

To summarize, samples tested, and hence effectively annealed, at temperatures greater than T_g have a greater degree of crystallinity and hence produced the cross-over of stress–strain curves.

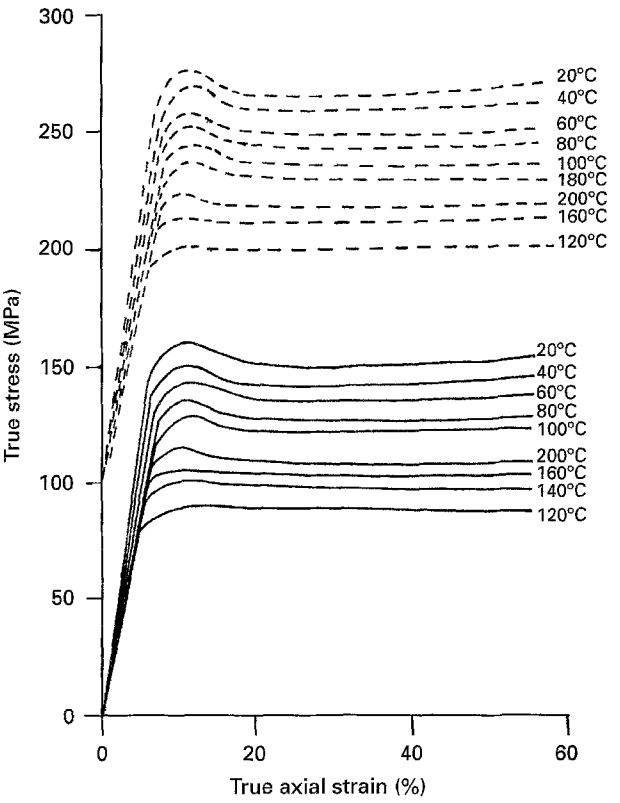

Figure 6 True stress against true axial strain for (——) PEEK and (- - - -) PEK from dropweight tests ($500\ s^{-1}$) at 20–200 °C. The PEK data have been offset by 100 MPa.

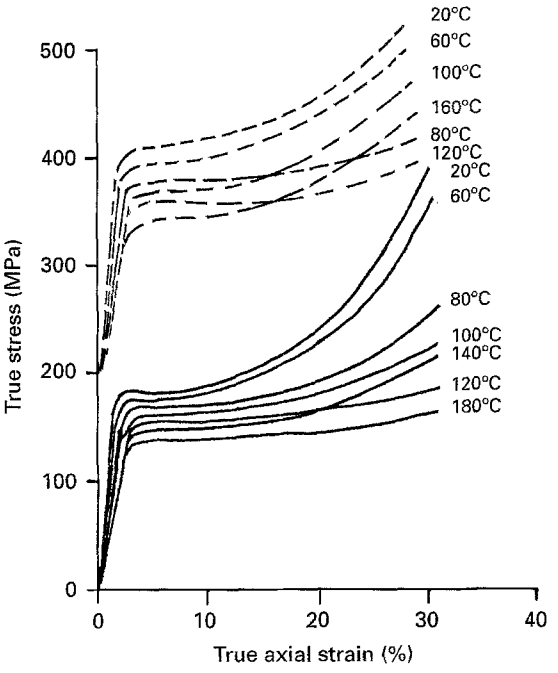

Figure 7 True stress against true axial strain for (——) PEEK and (- - - -) PEK from improved dropweight tests ($1000\ s^{-1}$) at 20–180 °C. The PEK data have been offset by 200 MPa.

3.2. X-ray analysis

After mechanical testing, we examined by wide-angle X-ray diffraction (WAXD) the tested samples and compared their patterns with those of annealed but untested samples. WAXD for PEEK and PEK annealed at different temperatures are shown in Figs 10

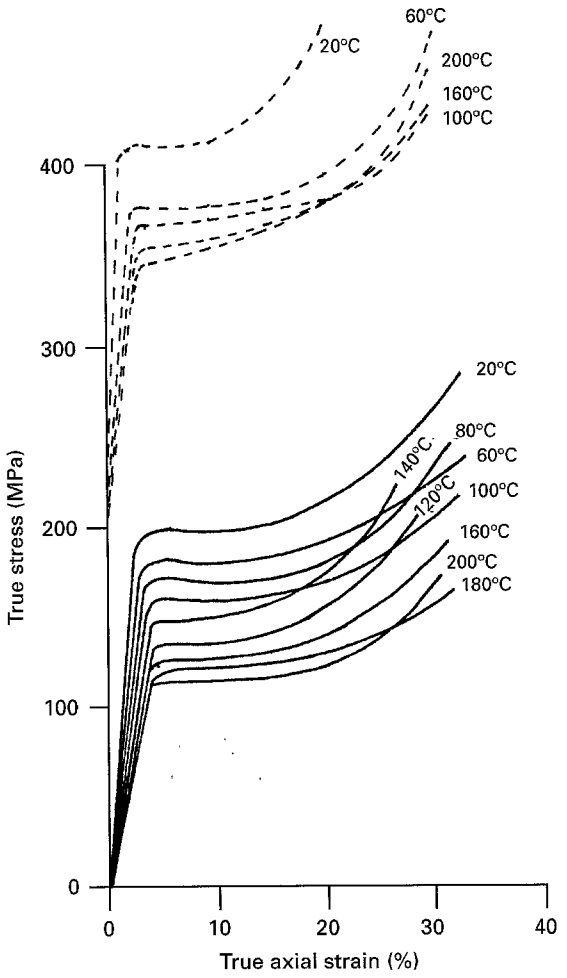

Figure 8 True stress against true axial strain for (——) PEEK and (----) PEK from cross-bow tests (2000 s^{-1}) at 20–200 °C. The PEK data have been offset by 200 MPa.

TABLE III Variation of yield stress with strain rate for PEEK and PEK at room temperature

Strain rate (s^{-1})	Yield stress PEEK (MPa)	Yield stress PEK (MPa)
3×10^{-3}	132 ± 5	150 ± 5
7	150 ± 5	170 ± 5
500	160 ± 5	176 ± 5
1000	190 ± 20	210 ± 20
2000	200 ± 10	214 ± 10

and 11. The crystal reflections from the annealed samples are similar throughout the various heat treatments. Although annealing temperature increases from 20 °C to 200 °C, the diffractograms showed that at all annealing temperatures, the untested samples contain the same volume fraction of crystallinity.

WAXD for the tested samples showed an apparent loss of sharp distinct crystalline reflections, as also shown in Figs 10 and 11. The high testing temperature diffractograms were more crystalline with broad reflections centred at scattering angles of 22° and 19° and had a less-amorphous background. These reflections increase with the annealing temperature. Although annealing produces the same volume fraction of crystallinity, as evinced from Figs 10 and 11, the tested samples showed that the crystallinity level in

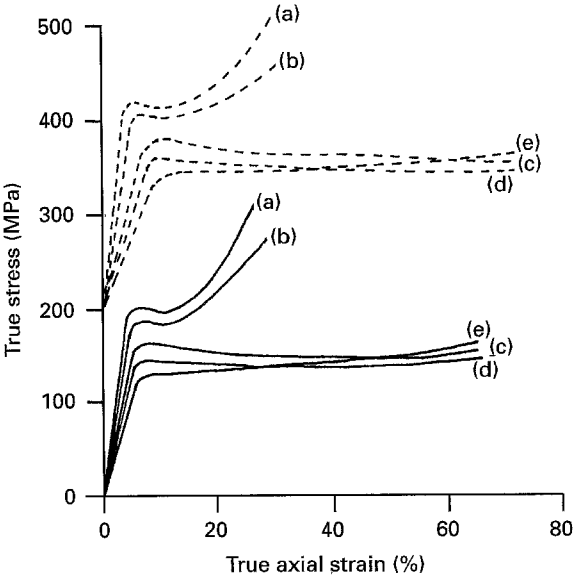

Figure 9 True stress against true axial strain for (——) PEEK and (----) PEK at 20 °C tested at five different strain rates. The PEK data have been offset by 200 MPa. Strain rates: (a) 2000 s^{-1}, (b) 1000 s^{-1}, (c) 500 s^{-1}, (d) 7 s^{-1}, (e) 0.001 s^{-1}.

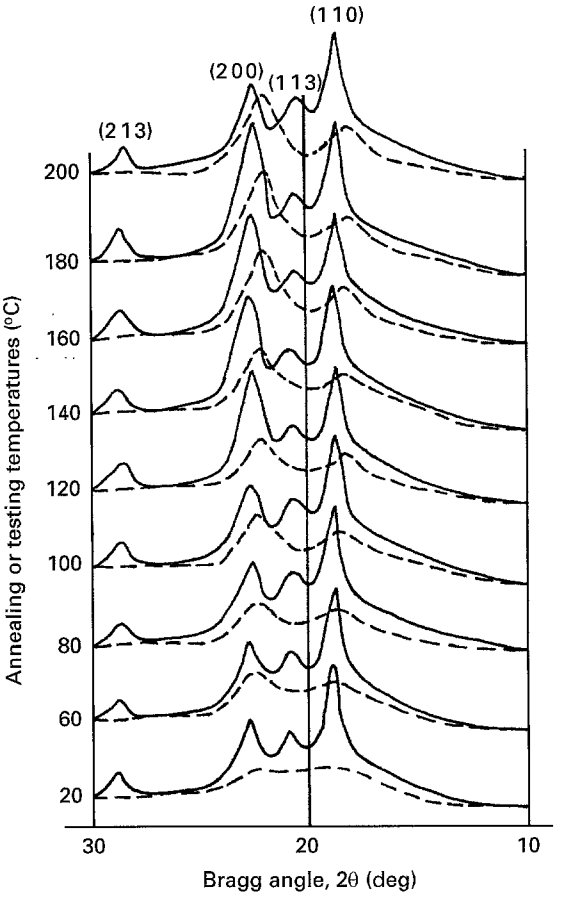

Figure 10 Diffractogram of (——) annealed and (----) tested PEEK.

the samples after straining increased with temperature.

3.3. Thermal analysis

The effect of mechanical testing on the crystalline morphology is reflected by the change of the thermal characteristics of the samples, as revealed by the DSC

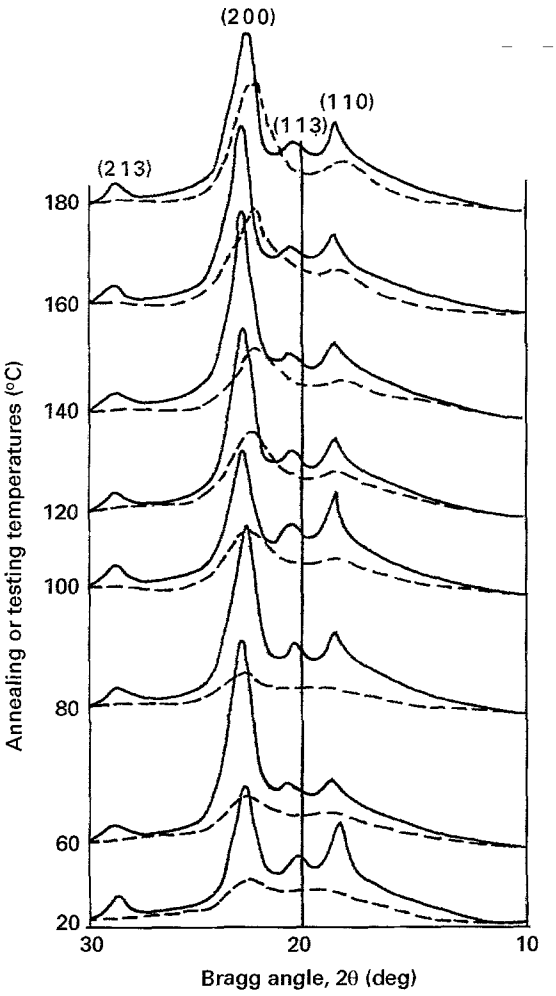

Figure 11 Diffraction of (——) annealed and (----) tested PEK.

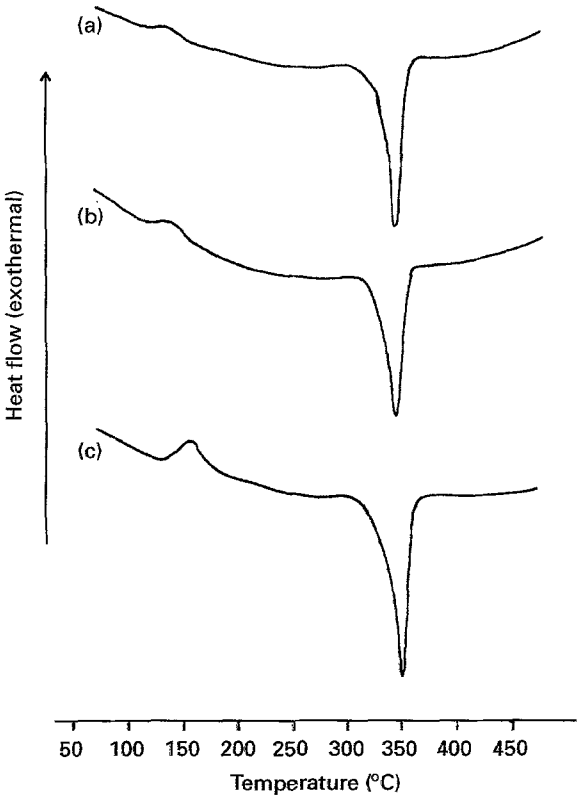

Figure 12 Thermograms of PEEK at room temperature, (a) as-received, (b) tested at $10^{-3}\,s^{-1}$ and (c) tested at $1000\,s^{-1}$.

TABLE IV Variation of melting endotherm for annealed and tested PEEK and PEK with temperature

Temperature (°C)	Melting endotherm					
	PEEK ($J\,g^{-1}$)			PEK ($J\,g^{-1}$)		
	Annealed	Tested		Annealed	Tested	
		.003 s^{-1}	1000 s^{-1}		.003 s^{-1}	1000 s^{-1}
20	50	37	56	57	55	62
60	42	45	56	52	53	66
80	44	46	58	56	52	65
100	52	44	62	54	53	65
120	50	43	62	57	54	67
140	47	50	63	57	49	71
160	50	41	60	51	52	69
180	49	43	59	57	54	66

technique (see Fig. 12). Table IV shows the melting endotherms of the PEEK and PEK samples annealed and tested at different temperatures and strain rates. It is found that the total crystallization content of the samples tested at high strain rate is higher than that of annealed samples.

At low strain rates ($3 \times 10^{-3}\,s^{-1}$), the DSC scans show cold crystallization over the whole range of testing temperatures. Cold crystallization can be attributed to the recrystallization during the heating run, which agrees with the proposal of Blundell [12]. These scans show that no crystallization occurs even at the higher temperatures during low strain-rate tests. Therefore, hardening due to crystallization does not occur. For this reason the cross-over of stress–strain curves in which the yield stress at 120 °C is less than that at 140 °C does not occur in the low strain-rate test.

At higher strain rates ($10^{3}\,s^{-1}$), only samples tested at lower temperatures show cold crystallization. From the DSC scans it appears that only samples tested below T_g undergo cold crystallization. This indicates that mechanical testing of the annealed semicrystalline samples at higher strain rates and above T_g results in the increase of the crystal structure.

3.4. Discussion and conclusion

Changes in both the rate of loading and temperature have been used to produce a series of stress–strain curves. This comprehensive set of curves can be used to gain an understanding of the time and temperature dependences of material mechanical properties. Increasing strain rate increases the yield stress, but the process becomes adiabatic and the resulting temperature increase can reduce the flow stress at higher strains.

When comparing the stress–strain curves from the five strain-rate tests (Fig. 9), there is an apparent sign of transition from the isothermal to adiabatic processes. For quasi-static tests, both PEEK and PEK showed strain hardening after yield. At 7 and $500\,s^{-1}$, both curves showed strain softening after yield. This is due to adiabatic heating during the test which lowers the flow stress. Hall [13] has shown that this heating is

important for tests conducted at rates above $4\,s^{-1}$. Tests conducted at $1000\,s^{-1}$ and above show a significant increase in yield and flow stress. It may be suspected that this is due to inaccuracies in the measuring equipment. However, because the results obtained originate from two totally independent sets of apparatus working on different measurement principles, the increase is believed to be genuine.

The strain–rate sensitivity can be determined from the stress against log strain rate plots. Both PEEK and PEK exhibited a bilinear relationship between the stress and log strain rate where the strain–rate sensitivity increases sharply at a strain rate of about $500\,s^{-1}$. For strain rates up to $500\,s^{-1}$ the strain–rate sensitivity for PEEK at 20 °C is 3–5 MPa per decade of strain rate, while at 100 °C the value drops to 2–4 MPa per decade of strain rate (Figs 13 and 14).

The strain–rate sensitivities for PEK at 20 and 100 °C are 3–5 and 3–6 MPa per decade of strain rate, respectively (Figs 15 and 16). It can be concluded that up to 100 °C the strain–rate sensitivity of PEK is not sensitive to the increase in temperature. For simplicity, the average strain–rate sensitivity for both PEEK and PEK at a strain rate below $500\,s^{-1}$ is taken as 4 MPa per decade of strain rate. Strain hardening occurred as the strain rate was raised from $500\,s^{-1}$ to $1000\,s^{-1}$ for both PEEK and PEK. The strain–rate sensitivities obtained at a strain rate greater than $500\,s^{-1}$ for both PEEK and PEK are 60 MPa per decade of strain rate, that is ten times higher than the strain–rate sensitivity obtained at strain rate below $500\,s^{-1}$.

An Eyring equation

$$\frac{\sigma}{T} = \frac{\Delta H}{V_A T} + \frac{R}{V_A} \ln \frac{2\dot{\varepsilon}}{\dot{\varepsilon}_0} \qquad (1)$$

relating stress with the strain and strain rate, is used to model the constitutive relationship. The straight line obtained by plotting σ_y/T against log strain rate for both PEEK and PEK is in accordance with the prediction of Eyring theory (see Figs 17 and 18). It is found that the Eyring theory was obeyed well for five decades of strain rate (10^{-3}–$10^{2}\,s^{-1}$) for temperatures up to 120 °C but breaks down at higher rates. Figs 19 and 20 show a plot of $\sigma_{20\%\varepsilon}/T$ against log strain rate for PEEK and PEK, respectively. Above 120 °C, both PEEK and PEK showed a decrease in σ_y/T and $\sigma_{20\%\varepsilon}/T$ when plotted against log strain rate.

Using a simple equation, i.e.

$$\sigma = \frac{KT}{V_A} \ln \frac{\dot{\varepsilon}}{\dot{\varepsilon}_0} \qquad (2)$$

and the average strain–rate sensitivity, i.e. 4 MPa per decade of strain rate, the calculated activation volumes for both PEEK and PEK are 1.0 nm^3. Alternatively the activation volume can also be calculated by equating the gradient of the slope in Fig. 17 to R/V_A

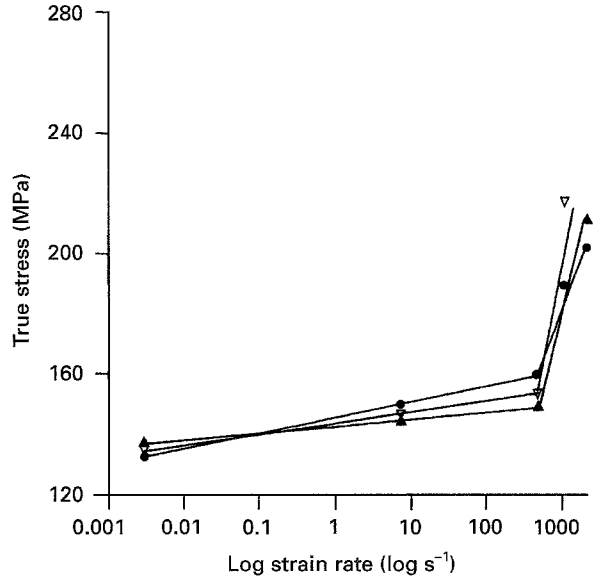

Figure 13 True stress against log strain rate for PEEK at 20 °C at (●) 10% (▽) 15%, and (▲) 20% strain.

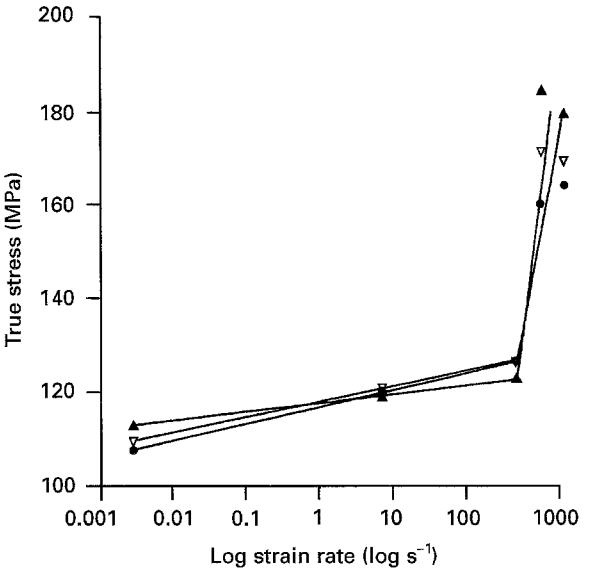

Figure 14 True stress against log strain rate for PEEK at 100 °C at (●) 10% (▽) 15%, and (▲) 20% strain.

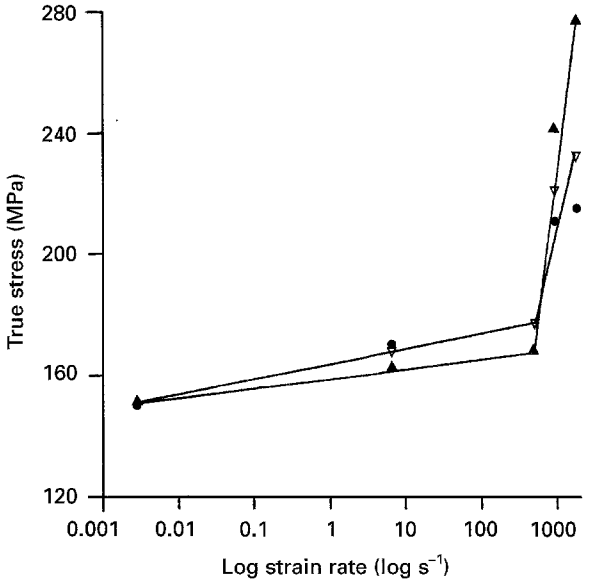

Figure 15 True stress against log strain rate for PEK at 20 °C at (●) 10% (▽) 15%, and (▲) 20% strain.

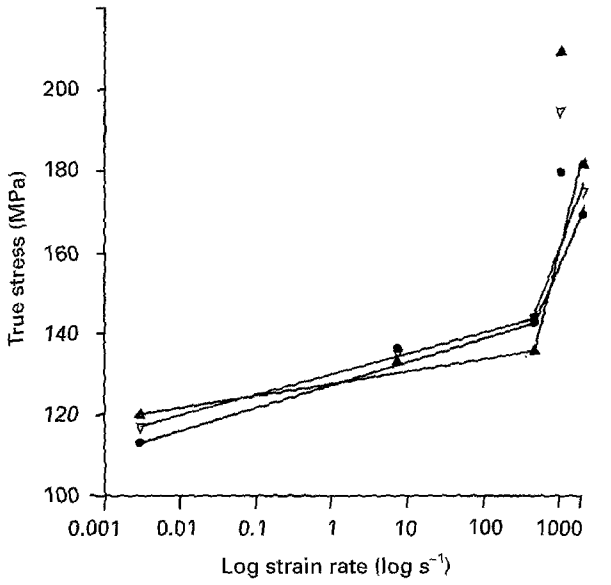

Figure 16 True stress against log strain rate for PEK at 100 °C at (●) 10% (▽) 15%, and (▲) 20% strain.

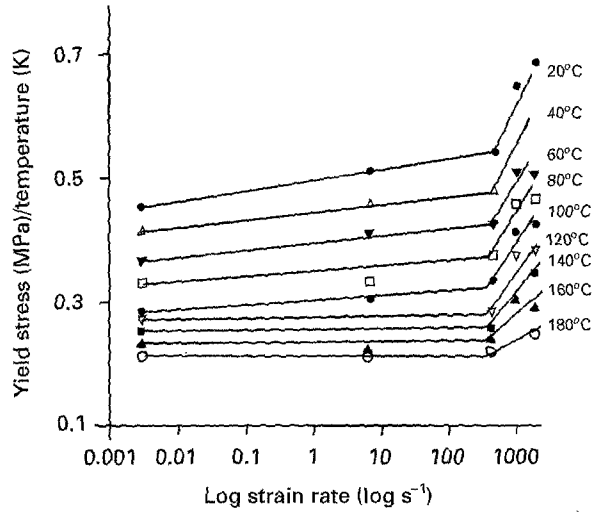

Figure 17 Yield stress/temperature versus log strain rate for PEEK at various temperatures.

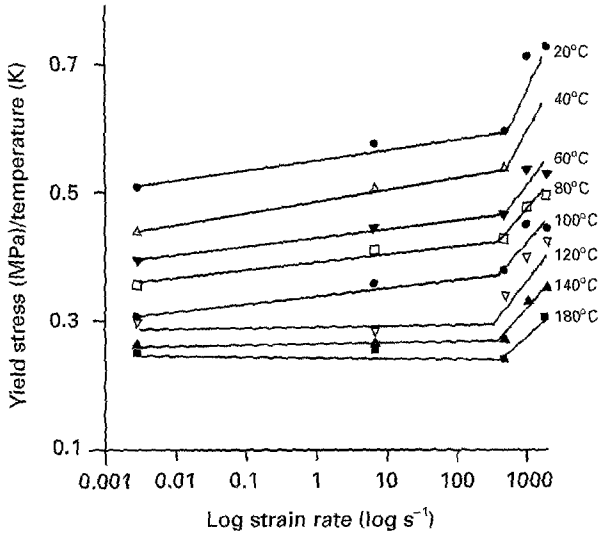

Figure 18 Yield stress/temperature versus log strain rate for PEK at various temperatures.

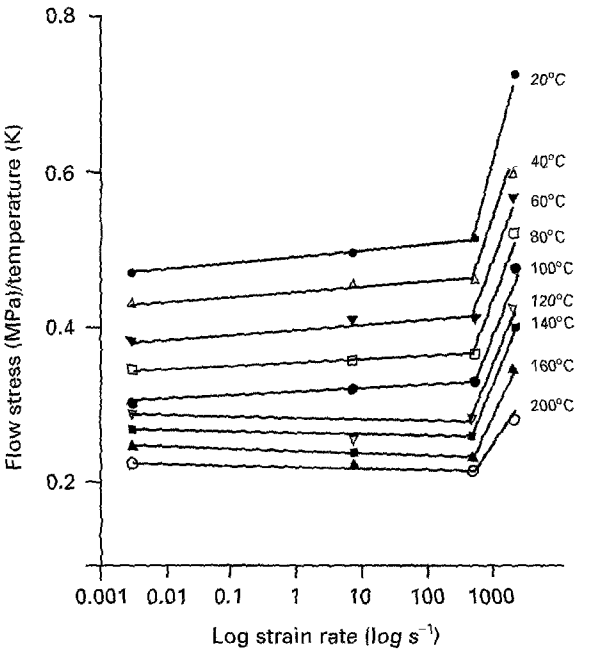

Figure 19 Flow stress at 20% strain/temperature versus log strain rate for PEEK at various testing temperatures.

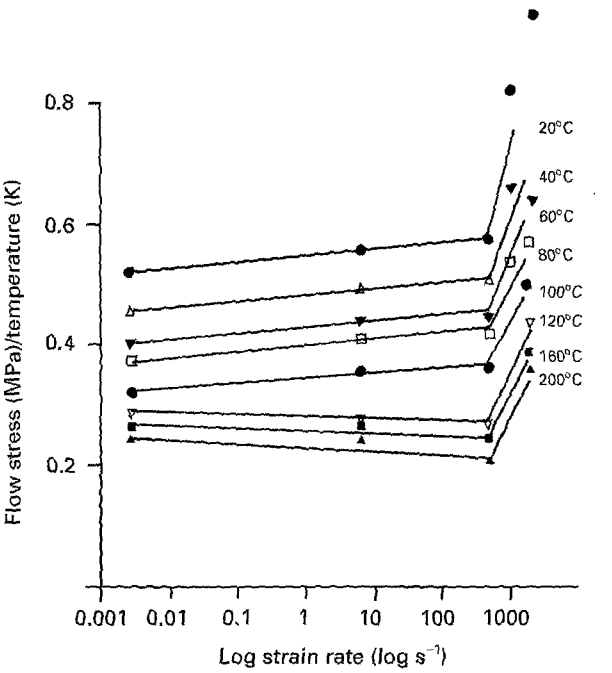

Figure 20 Flow stress at 20% strain/temperature versus log strain rate for PEK at various testing temperatures.

using Equation 1. This leads to an activation volume of 0.8 nm^3. These values are in good agreement with the finding of Dawson [14] and the activation volume for other polymers as shown in Table 11.1 of [15].

In the range of strain rates studied, there is an obvious transition from isothermal to abiabatic processes observed in the stress–strain curves although not easily observed in the stress–log strain-rate plot due to lack of data at a range of low strain rates. Results obtained at various strain rates showed that the cross-over of the stress–strain curves at certain strain rates (i.e. 7 and 500 s^{-1}) is due to thermal

TABLE V Calculated temperature rise (ΔT) with strain rate ($\dot{\varepsilon}$) at various strain (10%, 15% and 20% ε)

$\dot{\varepsilon}$ (s^{-1})	$\Delta T_{10\%\varepsilon}$ (°C)	$\Delta T_{15\%\varepsilon}$ (°C)	$\Delta T_{20\%\varepsilon}$ (°C)
7	7	15	24
500	7	16	26
1000	11	19	28
2000	9	19	26

softening caused by adiabatic processes. These correspond to an increase in the temperature of the sample. Table V shows the temperature rise during deformation calculated by integrating under the stress–strain curves. At higher strain rates (10^3 s^{-1}) strain hardening reappears. Although the process is adiabatic, the fast rate causes the polymer to become brittle.

In the range of temperature studied, it is clear that a major change occurs on passing through the glass transition temperature, despite the presence of the crystalline fraction. This transition is obviously related to the glass transition of the semicrystalline polymers and cold crystallization which occurs with greater molecular mobility around the glass transition. Increasing the temperature up to T_g obviously reduces the polymer strength, but above T_g the effect of crystallinity can strengthen the polymer significantly. Because below T_g the amorphous component is in a glassy state, the flow stress decreases with increase in temperature. Above T_g, this behaviour strongly depends on the degree of crystallinity. For tests above T_g, we see that an increased degree in crystallinity results in an increase in flow stress.

Investigations into the behaviour around T_g were done using WAXD and DSC. Both techniques showed that increasing the annealing temperature in the absence of strain produced only slight increases in the degree of crystallinity. The results are wholly satisfactory for comparative purposes. It is clear that changing the test temperature produces different degrees of crystallinity in both polymers studied, as determined by WAXD. These changes again occur in the way in which we would expect from the DSC results, namely that the crystallinity is associated with the cross-over of the stress–strain curves in the high strain-rate testing. The increase in crystallinity due to recrystallization at elevated temperatures causes an increase in the flow stress for testing above T_g.

The results based on thermal analysis indicate that the presence of secondary crystallites, with a low degree of stability, may also have a direct effect on the flow stress. The increase in the melting endotherm on increasing the annealing temperature means that at higher temperature, the number of chains able to crystallize increases and more perfect crystals are formed. The increase in crystallinity might involve an increase in the total number of crystallites or the average perfection of existing crystallites.

Acknowledgement

The authors acknowledge the provision of financial support for the work described in this paper from the UK Science and Engineering Research Council (now EPSRC) under grant GR/F45073.

References

1. T. E. ATTWOOD, P. C. DAWSON, J. L. FREEMAN, L. R. J. HOY, J. B. ROSE and P. A. STANILAND, *Polymer* **22** (1981) 1096.
2. S. Z. D. CHENG, M. Y. CAO and B. WUNDERLICH, *Macromolecules* **19** (1986) 1868.
3. P. C. DAWSON and D. J. BLUNDELL, *Polymer* **21** (1980) 577.
4. D. R. RUEDA, F. ANIA, A. RICHARDSON, I. M. WARD and F. J. BALTA CALLEJA, *Polym. Commun.* **24** (1983) 258.
5. D. J. BLUNDELL and B. N. OSBORN, *Polymer* **24** (1983) 953.
6. P. CEBE and S. D. HONG, *ibid.* **27** (1986) 1183.
7. C. N. VELISARIS and J. C. SEFERIS *Polym. Eng. Sci.* **28** (1988) 583.
8. L. H. LEE, J. J. VANSELOW and N. S. SCHNEIDER, *ibid.* **28** (1988) 181.
9. S. M. WALLEY, J. E. FIELD, P. H. POPE and N. A. SAFFORD, Philos. Trans. R. Soc. Lond. **A328** (1989) 1.
10. J. E. FIELD, G. M. SWALLOWE, P. H. POPE and S. J. P. PALMER, "Mechanical Properties at High Rates of Strain", Institute of Physics Conference Series 70 (IPC, London 1984) pp. 381–8.
11. D. A. GORHAM, "Mechanical Properties at High Rates of Strain", Institute of Physics Conference Series 47 (ICP, London, 1979) pp. 16–24.
12. D. J. BLUNDELL, *Polymer* **28** (1987) 2248.
13. I. H. HALL, *J. Appl. Polym. Sci.* **12** (1968) 739.
14. P. C. DAWSON, PhD thesis, Loughborough University (1993).
15. I. M. WARD, "Mechanical Properties of Solid Polymers", 2nd Edn (Wiley, 1979).

Received 23 January
and accepted 7 November 1995